Maximum entropy regularization of the geomagnetic core field inverse problem

Andrew Jackson,[1] Catherine Constable[2] and Nicolas Gillet[3]

[1]*Institut für Geophysik, ETH Zürich, CH-8093, Switzerland*
[2]*IGPP, Scripps Inst. of Oceanography, La Jolla 92093 CA, USA*
[3]*School of Earth and Environment, University of Leeds, Leeds LS2 9JT, UK. E-mail: earng@earth.leeds.ac.uk*

SUMMARY

The maximum entropy technique is an accepted method of image reconstruction when the image is made up of pixels of unknown positive intensity (e.g. a grey-scale image). The problem of reconstructing the magnetic field at the core–mantle boundary from surface data is a problem where the target image, the value of the radial field B_r, can be of either sign. We adopt a known extension of the usual maximum entropy method that can be applied to images consisting of pixels of unconstrained sign. We find that we are able to construct images which have high dynamic ranges, but which still have very simple structure. In the spherical harmonic domain they have smoothly decreasing power spectra. It is also noteworthy that these models have far less complex null flux curve topology (lines on which the radial field vanishes) than do models which are quadratically regularized. Problems such as the one addressed are ubiquitous in geophysics, and it is suggested that the applications of the method could be much more widespread than is currently the case.

Key words: core magnetic field, geomagnetic inverse problem, geomagnetic modelling, maximum entropy.

1 INTRODUCTION

The interpretation of a data set in terms of interesting properties of the Earth is a long-standing activity in geophysics. The Earth supplies data, via the experiment, through the so-called 'forward problem', and deficiencies in the experiment along with approximations in theory (including unmodelled signals) and random sources of error add noise to the data set. Almost all interpretations require that the individual solve a so-called inverse problem, namely inferring properties of the earth model **x** from the data γ. Apart from a handful of problems where the interesting parameters governing the system are finite in number, most problems involve an Earth model which is a continuous function of the independent parameter (say time, position in one, two or three dimensions, or both), and thus the Earth model is strictly infinite dimensional. Even in the case of a linear forward problem, since the work of Backus & Gilbert (1967) it has been known that such problems are fundamentally non-unique, and their solutions require the injection of prior information into the problem.

In a similar vein, it is possible to group the methodologies for the solution of inverse problems into two categories: probabilistic and non-probabilistic. Whilst there are certainly commonalities between the approaches, and indeed identical final calculations often result (e.g. Backus 1988), there is a real distinction between them. In this paper, we will avoid the probabilistic approach, and instead follow the 'minimum structure' or 'minimum complexity' approach espoused by Parker (1994), which leads to calculations in which a conventional least-squares estimate of the model is 'regularized' by minimizing a chosen norm of the model; the approach is also termed penalized least-squares. However, the major thrust of this paper is to introduce a particular non-quadratic regularization method, the maximum entropy method, to models whose sign is unconstrained; this method has had some implementation previously to models which are known to be intrinsically positive, which is its normal application. With the exception of the electromagnetic inverse problem, where the positivity of the electrical conductivity usually plays a crucial role, very few models in geophysics are set up such that the positivity plays an important role: either the logarithm of the quantity on question is the natural quantity to seek (e.g. viscosity in the mantle), or the problem is more usually set relative to a reference model, and perturbations of unconstrained sign are sought (e.g. seismic tomography).

Much of the requisite theory for models which are intrinsically positive by design has been developed in the image recovery literature, with applications in astronomy and medical physics fields, as well as spectroscopy, X-ray crystallography and nuclear magnetic resonance; the interested reader should consult Buck & Macaulay (1991) for a lucid introduction to the subject. There has been some development of the theory to treat image recovery where there is no intrinsic positivity; this appears first in Gull & Skilling (1990), and is further developed in Hobson & Lasenby (1998). An excellent exposition of the subject can be found in Sivia & Skilling (2006), which is highly recommended. An example of how the method follows logically from known physical approximations applied to the

GJI Geomagnetism, rock magnetism and palaeomagnetism

geomagnetic inverse problem of reconstructing the core magnetic field was sketched in Jackson (2003).

Our paper is accompanied by a companion paper, Gillet *et al.* (2007), hereinafter Paper II, which applies the method to time-dependent field modelling, and also develops the method within the much more familiar setting of spherical harmonic analysis. Here we develop the basic theory of the approach and provide synthetic test cases in order to compare performance with other techniques. Thus, this paper sets up much of the groundwork required for Paper II.

The arrangement of the paper is as follows. Section 2 introduces the basic maximum entropy (Maxent) method, applicable to positive images. Section 3 shows how this can be modified to treat models that are not intrinsically positive. Section 4 applies the method to the geomagnetic inverse problem, giving a comparison between results obtained using a maximum entropy method and those obtained by traditional methods.

2 THE CANONICAL LINEAR INVERSE PROBLEM

The core-field inverse problem can be posed in the form of a linear inverse problem when Cartesian components of the magnetic field **B** are measured, so let us consider the following canonical inverse problem: let γ be a vector of measurements $\{\gamma_i: i = 1, N\}$, related to an underlying earth model **x**: $\{x_i: i = 1, P\}$ via a design matrix **A**:

$$\gamma = \mathbf{A}\mathbf{x}. \tag{1}$$

We are interested, in particular, in positive additive distributions, or PADs (we will dispense with this specialization later); such distributions commonly occur as images in both the visible and radio ranges (where the addition of photons to a pixel increases the intensity of the image proportionally) and in spectroscopy, nuclear magnetic resonance, X-ray tomography and small angle neutron scattering.

As a general rule, the reconstruction problems are ill posed and underdetermined, in the sense that either $N < P$ or the condition number of **A** is very large. Such problems require a way of selecting solutions from the otherwise huge selection of models fitting the data; a typical method of approach is that of regularization, picking a model which optimizes some particular characteristic.

We proceed to solve the problem in this way by adding prior information (regularization); in the case of noisy data where the noise is independent and identically distributed, originating from a Gaussian distribution with variance σ^2, we have to solve the following schematic problem:

$$\text{Minimize} \left\{ \sum_{i=1}^{N} \left[\frac{(\gamma_i - \tilde{\gamma}_i)}{\sigma^2} \right]^2 + \lambda \mathcal{R}(\mathbf{x}) \right\} = \chi^2 + \lambda \mathcal{R}(\mathbf{x}), \tag{2}$$

where $\tilde{\gamma}_i$ is the model prediction of the ith datum. The regularization is $\mathcal{R}(\mathbf{x})$, discussed below, and λ is a damping/regularization parameter, chosen to obtain a sensible fit of the data (here in terms of the chi-squared measure) to the model (see Parker 1994, for a discussion of acceptable levels of fit).

In geophysics, in particular, much attention has been given to regularizations based on quadratic measures of complexity; many examples are given in Parker (1994). A typical quadratic norm might be written in the form

$$N_Q = (\mathbf{x} - \mathbf{x}_0)^T \mathbf{\Lambda} (\mathbf{x} - \mathbf{x}_0) \tag{3}$$
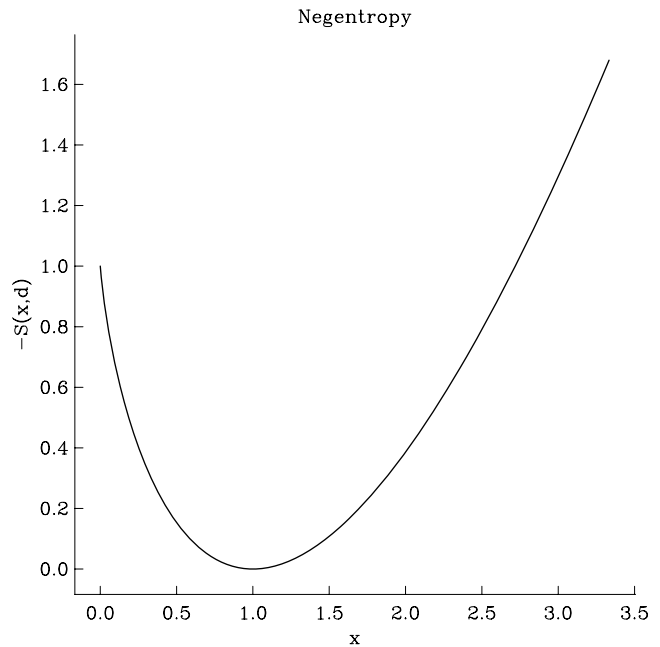
Figure 1. The negentropy $- S(x, d)$ for a single positive parameter. The default d has been set to unity.

for a given non-negative definite matrix $\mathbf{\Lambda}$ and an *a priori* model $\mathbf{x}_0$ (see Tarantola & Valette 1982a,b; Tarantola 1987). It should be recognized that this prior model (or 'default model', to use the parlance that is used below), from which deviations are measured under the two-norm, always needs to be specified. In many cases it is taken to be the zero model, though in some cases there are sensible default models, such as in seismology where a 1-D model (such as PREM) might be used when deriving a 3-D model.

An alternative approach, popular in disciplines where it is recognized that the underlying image is a PAD, is to maximize the entropy S of the image; we will not repeat the arguments here as to why the entropy S is a good property to maximize, which can be found in many sources; particularly recommended are Sivia & Skilling (2006) and Jaynes (2003).

When one demands that S be normalized, the entropy is given by

$$S(\mathbf{x}, \mathbf{d}) = \sum_{i=1}^{P} \left[x_i - d_i - x_i \log(x_i/d_i) \right], \tag{4}$$

where d_i is the 'default' for cell i. Fig. 1 shows the form of $-S$, termed the negentropy, which has a single unique minimum (at $x = d$). This shows the role of d: it is the value that each cell obtains in the absence of any data. In the application described here, all the d_i are set equal, as there is no *a priori* reason to set them otherwise. In this case, when there are no data, the image becomes the so-called 'flat map'. An important property of the MaxEnt solution is that it introduces no correlation at all between the pixels, other than that required by the data. For this reason it has known properties which can be thought of as undesirable in certain settings: for example, the problem of interpolation of a set of data on the line (see e.g. section 2.07 of Parker 1994 and section 6.3.1 of Sivia & Skilling 2006) has kernels linking the data to the underlying function that are singular. As a result of the lack of correlation induced by the MaxEnt solution, this problem has a solution that is composed of a set of spikes that satisfy the data points, not a solution that looks plausible to most observers (who have an in-built bias regarding the 'simplicity' of the solution).

We alert the reader here to the fact that there are shortcomings in the use of the entropy as a true prior probability density function (pdf) in a Bayesian framework. The problem lies in the fact that there is no pdf associated with the entropy that behaves properly in the continuum limit (see Skilling 1998). Therefore, in common with other authors, we eschew the Bayesian approach and simply use the entropy in the form of a regularizing function.

## 3 MODIFICATIONS FOR MODELS OF UNCONSTRAINED SIGN

It is the case that often the underlying models we seek are not themselves PADs, and it would appear that we cannot invoke maximum entropy as a way of choosing between models. However, actually a redefinition of the model still allows MaxEnt to play a role, and this section explains how.

In this section, in order to fix ideas, we will focus the arguments on the geomagnetic inverse problem of reconstructing the core magnetic field at the core–mantle interface based on measurements taken at or above the Earth's surface. We approximate the mantle as an insulator. Then measurements γ_i of the magnetic field are related to the field at the core–mantle boundary (CMB) $B_r(\theta, \phi)$ by linear relations of the form

$$\gamma_i = \int_\Omega G_i B_r \, d\Omega, \tag{5}$$

where G_i are known kernels (Gubbins & Roberts 1983; Backus *et al.* 1996). Fig. 2 shows the kernel for vertical measurements of the field. These kernels are the equivalent of the point-spread function in astronomy, and thus the deconvolution problem of reconstructing B_r is very severe.

For the problem at hand, where the underlying image (B_r) is not a PAD, we can still define the general radial core field B_r in terms of two spatially varying intensities B_r^+ and B_r^- (both of which must be
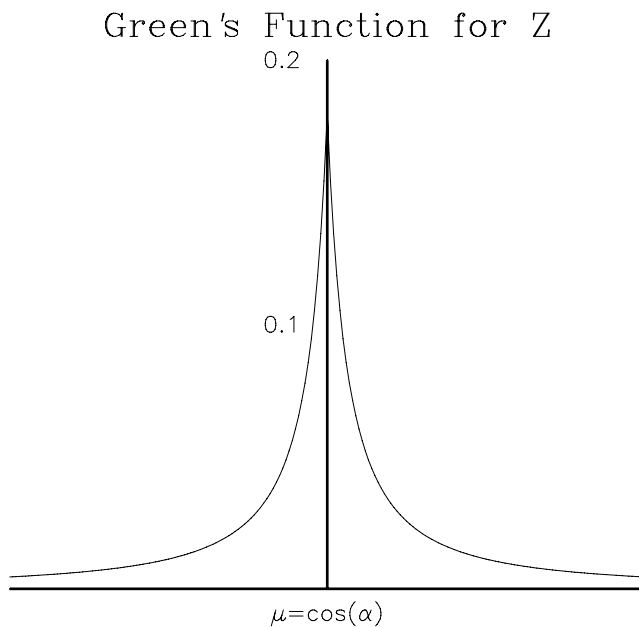
Figure 2. The kernel G_i as a function of cosine of angular distance α from the observation point for a vertical measurement of the core field made at the Earth's surface. The kernel is invariant with respect to rotation about the observation point.

positive) as $B_r = B_r^+ - B_r^-$. The problem is to reconstruct the two positive intensities B_r^+ and B_r^- from the surface data.

One can certainly solve this problem using a model of the core (the 'image') which consists of pixels with fluxes x_i^+ and x_i^-; a useful alternative is developed below. Fortunately, in the present geomagnetic problem, such a localized representation was developed by Constable *et al.* (1993), and this is the representation we adopt for the calculations. The representation is not strictly a pixel-based one, as there is in fact some overlap between the span of the basis functions. However, the resolution can be increased to a level that this becomes irrelevant, and the solution becomes the true maximum entropy one.

One can now see how the maximum entropy method enters the problem, since we now have two PADs to reconstruct. One maximizes the entropy, subject to fitting χ^2/N to unity with N data. (It is more rigorous to remove the number of degrees of freedom F in the model estimate from N in the denominator, though in the core-field reconstruction problem $N \gg F$ by several orders of magnitude, so this level of accuracy hardly seems justified.) The entropies enter the problem in terms of their sum, for the following reason. In reality we have a size $2P$ model $\mathbf{x} = (\mathbf{x}^+ | \mathbf{x}^-)^T$ to which the data are related by

$$\gamma = \mathbf{E}\mathbf{x} \tag{6}$$

with $\mathbf{E} = (\mathbf{A} | -\mathbf{A})$ from (1). Hence the entropy of the $2P$-vector $\mathbf{x}$ (whose components are intrinsically positive) is the sum of the entropies of the component P-vectors $\mathbf{x}^+$ and $\mathbf{x}^-$. Our optimization problem becomes

$$\text{Minimize}_{\substack{\mathbf{x}^+ > \mathbf{0} \\ \mathbf{x}^- > \mathbf{0}}} \{\chi^2 - \lambda[S(\mathbf{x}^+, \mathbf{d}^+) + S(\mathbf{x}^-, \mathbf{d}^-)]\}, \tag{7}$$

with λ chosen so as to achieve the required data fit, and S is the entropy given by (4). We have allowed for the possibility of two different defaults, $\mathbf{d}^+$ and $\mathbf{d}^-$, in (7); in everything that follows we take all elements of both of these defaults to be equal to a single scalar d. Because we pose (7) as a minimization problem, whilst we wish to maximize the entropy (subject to the data constraints), we instead introduce the negentropy $-S$ into the problem via the parameter λ. We note that an early example of this modification in crystallography, used to interpret X-ray powder diffraction data, has been given by David (1990).

The entropy as written in (4) is an approximation to the true value over the sphere. In principle, because it is impossible to tesselate the sphere uniformly, it should have some weight functions attached to each of the node values in the sum. Probably the correct weights would be the areas of the Voronoi cells (Sambridge *et al.* 1995) associated with each node. However, the fact that the STT parametrization does not give a true 'pixel'-based scheme, combined with the fact that the variation in the Voronoi cell size is tiny, means that we do not introduce this further complication.

3.1 Algorithms

We now turn to the issue of algorithms, because the maximization of a non-linear function such as the entropy is not a trivial matter; indeed, the construction of reliable algorithms attracted considerable effort during the 1980s. Much of the problem lies with the asymptotically infinite gradient of the entropy close to zero. Details of algorithms can be found in Skilling & Bryan (1984), or Gull & Skilling (1990). Fortunately for us, it turns out we can sidestep the issue of solving for two underlying images B_r^+ and B_r^- by solving

for their difference, provided we get the correct definition for the entropy of the difference. The following proof comes from Gull & Skilling (1990), though see also Hobson & Lasenby (1998); it is included to make the arguments self-contained.

We write **x** as the difference of two PADs **f** and **g**:

$$\mathbf{x} = \mathbf{f} - \mathbf{g}. \tag{8}$$

We assume **f** and **g** both have the same prior **d**, so that the total entropy can be written:

$$S(\mathbf{x}, \mathbf{d}) = S(\mathbf{f}, \mathbf{g}, \mathbf{d}) = \sum_i \left\{ f_i - d_i - f_i \log \left[\frac{f_i}{d_i} \right] \right\}$$
$$+ \sum_i \left\{ g_i - d_i - g_i \log \left[\frac{g_i}{d_i} \right] \right\}. \tag{9}$$

We may remove the explicit dependence of S on **f** and **g** by applying continuity constraints on S. Since $\mathbf{x} = \mathbf{f} - \mathbf{g}$ we have

$$\frac{\partial S}{\partial f_i} = \sum_k \frac{\partial S}{\partial x_k} \frac{\partial x_k}{\partial f_i} = \frac{\partial S}{\partial x_i}$$
$$\frac{\partial S}{\partial g_i} = \sum_k \frac{\partial S}{\partial x_k} \frac{\partial x_k}{\partial g_i} = -\frac{\partial S}{\partial x_i}, \tag{10}$$

so that

$$\frac{\partial S}{\partial f_i} + \frac{\partial S}{\partial g_i} = 0. \tag{11}$$

Some algebra (Gull & Skilling 1990) leads to the following conclusion for the form for S, free of the underlying fields **f** and **g**:

$$S(\mathbf{x}, \mathbf{d}) = \sum_{i=1}^{P} \left\{ \psi_i - 2d_i - x_i \log \left[\frac{\psi_i + x_i}{2d_i} \right] \right\}, \tag{12}$$

with

$$\psi_i = \sqrt{x_i^2 + 4d_i^2}. \tag{13}$$

The gradient

$$[\nabla S]_i = \log \left[\frac{\psi_i + x_i}{2d_i} \right] \tag{14}$$

and the Hessian

$$[\nabla\nabla S]_{ij} = \frac{1}{\psi_i} \delta_{ij} \tag{15}$$

are useful for the optimization.

Fig. 3 shows the form of the negentropy for an unsigned parameter, along with the quadratic approximation valid for small x (Maisinger *et al.* 1997); one can see that at large x the penalty is not so great from the negentropy as from quadratic regularization. One can implement this definition of the entropy in a very straightforward Newton-type algorithm, commonly used in non-linear geophysical problems. It is straightforward to implement the relevant derivatives in a conventional regularized solver of the form

$$\mathbf{x}^{k+1} = \mathbf{x}^k + \left(2\mathbf{A}^T\mathbf{C}_e^{-1}\mathbf{A} + \lambda\nabla\nabla S \right)^{-1} \left[2\mathbf{A}^T\mathbf{C}_e^{-1}(\gamma - \mathbf{A}\mathbf{x}^k) - \lambda\nabla S \right], \tag{16}$$

where $\mathbf{x}^k$ is the model vector at the kth iterate, and $\mathbf{C}_e$ is the error covariance matrix of the data, containing the variances of the errors on its diagonals in the simplest case of independent errors. Note that we have not employed step-length damping, though it is possible that it could be necessary; see Maisinger *et al.* (1997) for details. In the geomagnetic case the Newton-type solver of (16) converges rapidly when one starts from a nearby solution, and a quadratically regularized solution provides an excellent starting solution.
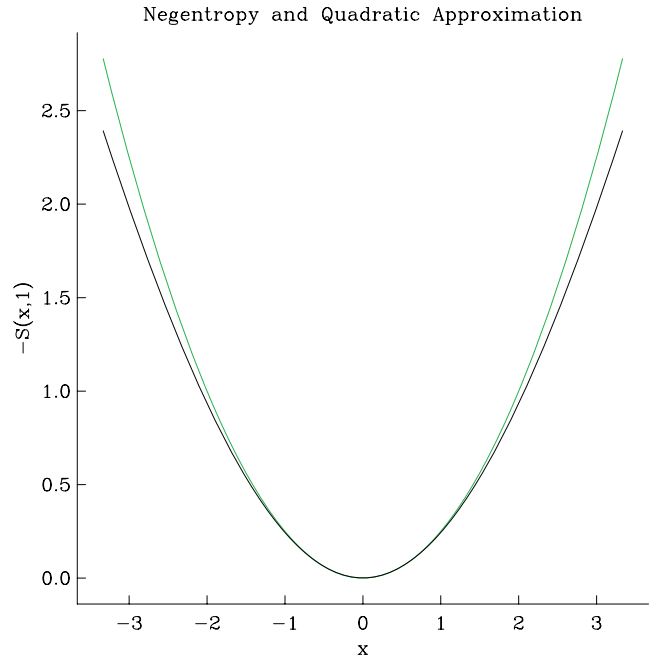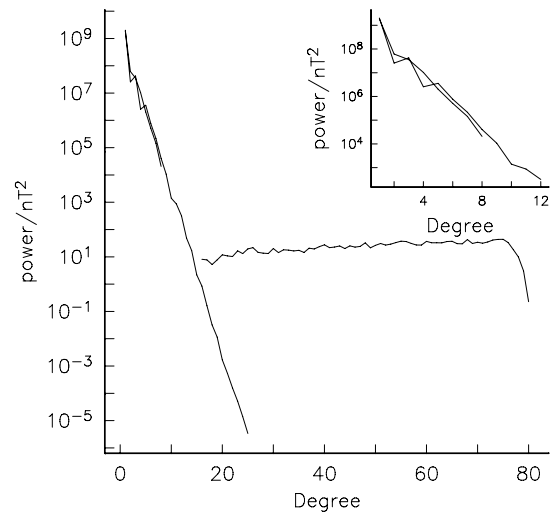

Figure 3. The negentropy $-S$ for an unsigned parameter. The default d has been set to unity. Also plotted as a green dashed line is the quadratic approximation, valid for $|x| \ll d$.

3.2 Implementation in LSQR

A very popular method for the solution of large tomographic systems is the method LSQR of Paige & Saunders (1982). In order that the maximum entropy method can be employed in such a scheme, perhaps for seismic tomography, we list here the simple modifications that are necessary. We can coax LSQR into solving the appropriate MaxEnt equations, if we pass to it the system

$$\begin{bmatrix} \mathbf{C}_e^{-1/2}\mathbf{A} \\ \mathbf{D} \end{bmatrix} \delta\mathbf{x} \approx \begin{bmatrix} \gamma - \tilde{\gamma} \\ \alpha \end{bmatrix}, \tag{17}$$


Figure 4. Dynamo model Lowes spectrum, MF2 Lowes spectrum and, for comparison, between degrees 1 and 8 the GSFC9/80 model evaluated in 1980. Inset shows the main field parts of the model in more detail. All are evaluated at the Earth's surface.

where $\mathbf{D} = \mathrm{diag}\{\sqrt{\lambda/\psi_i}\}$ and $\boldsymbol{\alpha} = -\sqrt{\lambda\psi_i}\nabla S$. This leads to the least-squares system

$$\left(\mathbf{A}^T\mathbf{C}_e^{-1}\mathbf{A} + \mathbf{D}^T\mathbf{D}\right)\delta\mathbf{x} = \mathbf{A}^T(\boldsymbol{\gamma} - \tilde{\boldsymbol{\gamma}}) + \mathbf{D}^T\boldsymbol{\alpha}, \qquad (18)$$

which can be verified to be the appropriate system. The implementation is then as follows.

(i) Calculate current predictions $\tilde{\boldsymbol{\gamma}}$ from the current model $\mathbf{x}^k$ at k^{th} iterate.

(ii) Set up $\mathbf{D}$ and $\boldsymbol{\alpha}$ from the current model $\mathbf{x}^k$.

(iii) Call LSQR to solve for $\delta\mathbf{x}$.

(iv) $\mathbf{x}^{k+1} = \mathbf{x}^k + \chi\,\delta\mathbf{x}$ (step length damping (using weight χ) may be implemented).
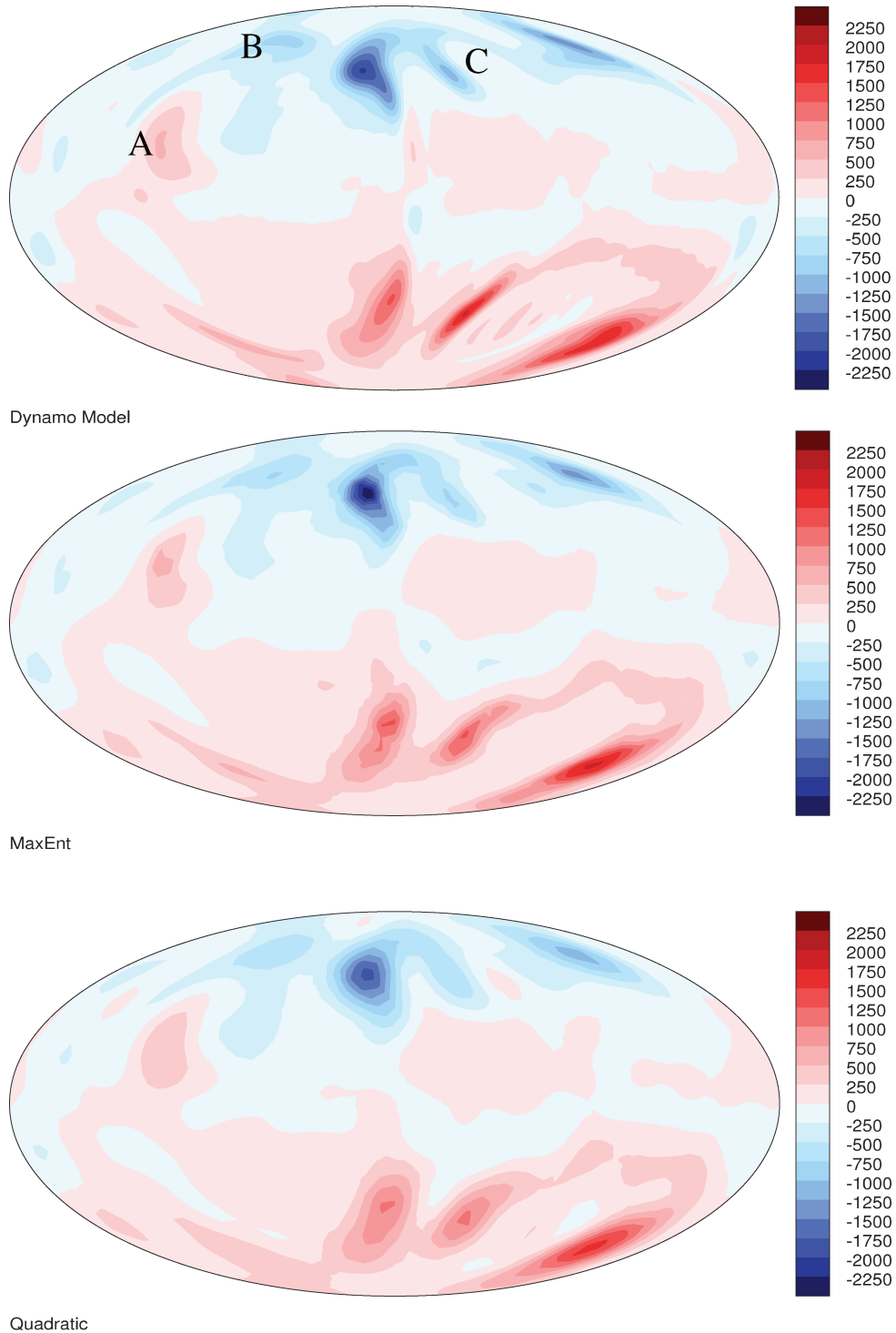
Figure 5. Comparison of the radial magnetic field from the original dynamo model with the output of the two inversion schemes, on Aitoff equal-area projection. Red colours represent magnetic flux out of the core, while blue colours represent magnetic flux entering the core; each colour bar represents an interval of 250 µT. At the top is the original dynamo field before contamination with the crustal field. In the middle is the result of the maximum entropy inversion, and at the bottom is the quadratic damping result.

(v) If step-length damping—find optimal χ.
(vi) Convergence? If not go again.

4 APPLICATION TO THE GEOMAGNETIC INVERSE PROBLEM

4.1 Application to a synthetic data set

In this section we implement the theory developed above in the geomagnetic inverse problem of reconstructing the radial magnetic field at the CMB based on observations taken at satellite altitude. A simulated data set is used in order that the results can be compared with a known input, in order to see the typical abilities of the method.

In the simulation we take the output from a numerical dynamo model kindly supplied by Ulrich Christensen. The dynamo was computed with an Ekman number of 10^{-3}, Prandtl number 1, magnetic Prandtl number 4, modified Rayleigh number 300 and rigid boundaries (see Christensen *et al.* 1999). When one computes an average magnetic Reynolds number it is 156, within the reasonable range for the Earth's core. The model is truncated at degree 42, and has a slowly decreasing spectrum at the CMB. We normalized the field model to give Earth-like amplitudes. We then add the field model MF2 of Maus *et al.* (2006), which represents the crustal spectrum from spherical harmonic degrees 16–80. The spectrum of the field models is plotted in Fig. 4. The model itself on the core surface is shown in Fig. 5. We use this model to synthesize 1600 Z measurements at the same sites as in the 1980 data set of Shure *et al.* (1985) at altitude 400 km, and we assign the data an error of 2.5 nT; this number is representative of the variance of the crustal field model that was added.

The representation of the core magnetic field for the inverse problem is in the form of the 'spherical triangle tesselation' (Constable *et al.* 1993) whereby the core is tesselated into $P = 1442$ almost equally spaced nodes and 2880 spherical triangles. The node structure is based on the subdivision of the regular icosahedron (Baumgardner & Fredrickson 1985). We invert the synthetic data set using both quadratic regularization, minimizing the norm

$$\mathcal{Q} = \int_{\Omega} B_r^2 \, d\Omega, \tag{19}$$

and with the maximum entropy method with default 10 μT, as was used in Jackson (2003). Both solutions are computed with misfit ($\sqrt{\chi^2/N}$) equal to unity; in order to obtain this value for the MaxEnt solution required that the damping parameter $\lambda = 0.05$; the model has negentropy $789 \times 10^3 \, \mu$T.

Examination of the results in Fig. 5 shows that the maximum entropy image is generally more in accord with the original. The quadratic solution, whilst being reasonably consistent, has been smoothed too much. In many places there appears to be about 1 contour interval of extra resolution in the MaxEnt image; these are most easily seen where the field is higher than average (e.g. pink patch A; blue patch B; blue 'tongue' of field C). One contour interval places an upper bound on the improvement, so it is certainly less than 250 μT.

In order to quantify these assertions, we have compared the results to the known 'truth', namely the values of the field on the CMB supplied by the original dynamo model. We calculated the differences between the estimate of B_r from the MaxEnt model at 6480 STT cell centres on the core surface (which originate from a 3242 node tesselation of the core); the results are shown in Fig. 6. The results have been computed using the technique described in Paper II,
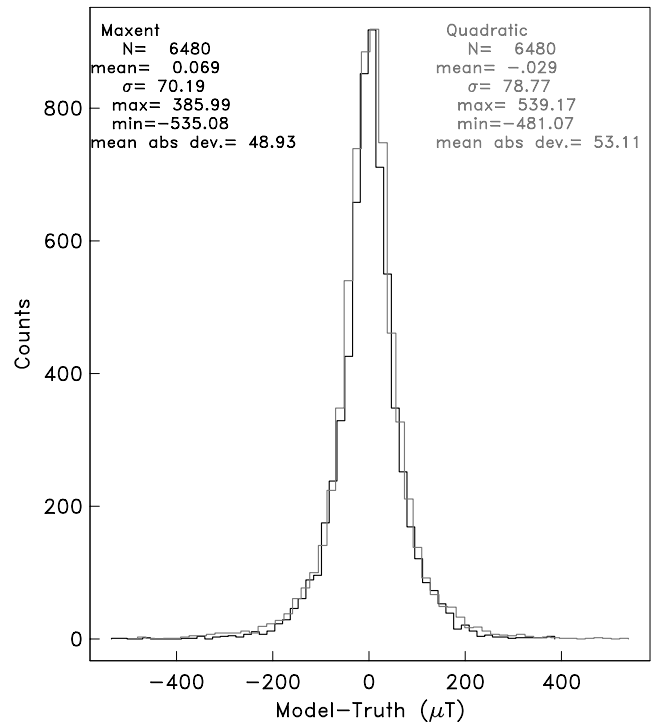

Figure 6. Comparison of the residuals (between model estimates and the known input) in the synthetic experiment, for MaxEnt (black) and quadratic (grey) regularization methods. In the text, N is the number of samples, σ is the standard deviation, max and min are the maximum and minimum of the residuals, and the 'mean abs dev.' is the mean of the absolute values of the residuals (all in μT). The MaxEnt model used $d = 10 \, \mu$T; even better performance of MaxEnt can be found when $d = 30 \, \mu$T (see text).

Table 1. Properties of the synthetic test results: tabulated are quadratic norm $\mathcal{Q}$, entropy S, unsigned flux $\mathcal{N}$ (see eq. 20), standard deviation σ and mean absolute deviation (MAD) of the differences between the model and the true model at 6480 cell centres on the core surface.

Model	$\mathcal{Q}$ (mT^2)	$\mathcal{N}$ (mT)	S (μT)	σ (μT)	MAD μT
MaxEnt	1.18	2.56	-789×10^3	70.2	48.9
Quadratic	1.15	2.68	-808×10^3	78.8	53.1

namely using the spherical harmonic adaptation of the method. The figure demonstrates that the improvement seen in Fig. 5 is real and quantifiable. The MaxEnt model has roughly a 10 per cent improvement in the standard deviation, and of the mean absolute deviation (70.2 μT versus 78.8 μT for σ and 48.9 μT versus 53.1 μT for the mean absolute deviation, for the MaxEnt and the quadratic models, respectively); see Table 1. The reason that the MaxEnt model appears better visually is that it has superior performance on the wings of the distribution, with fewer large residuals in the 200–400 μT range (see Fig. 6). It is of course these larger discrepancies that are most visible on a plot with contour intervals of 250 μT. Fig. 7 shows the spatial distribution of the differences between the model estimates and the true input model. The largest residuals are associated with the positions of high amplitude, and it is again clear that the Maximum entropy solution performs better than the quadratically regularized model.

Some words are in order regarding the default parameter d. It has been chosen completely arbitrarily to be 10 μT in the work described herein, consistent with the results previously reported in

(a)

(b)
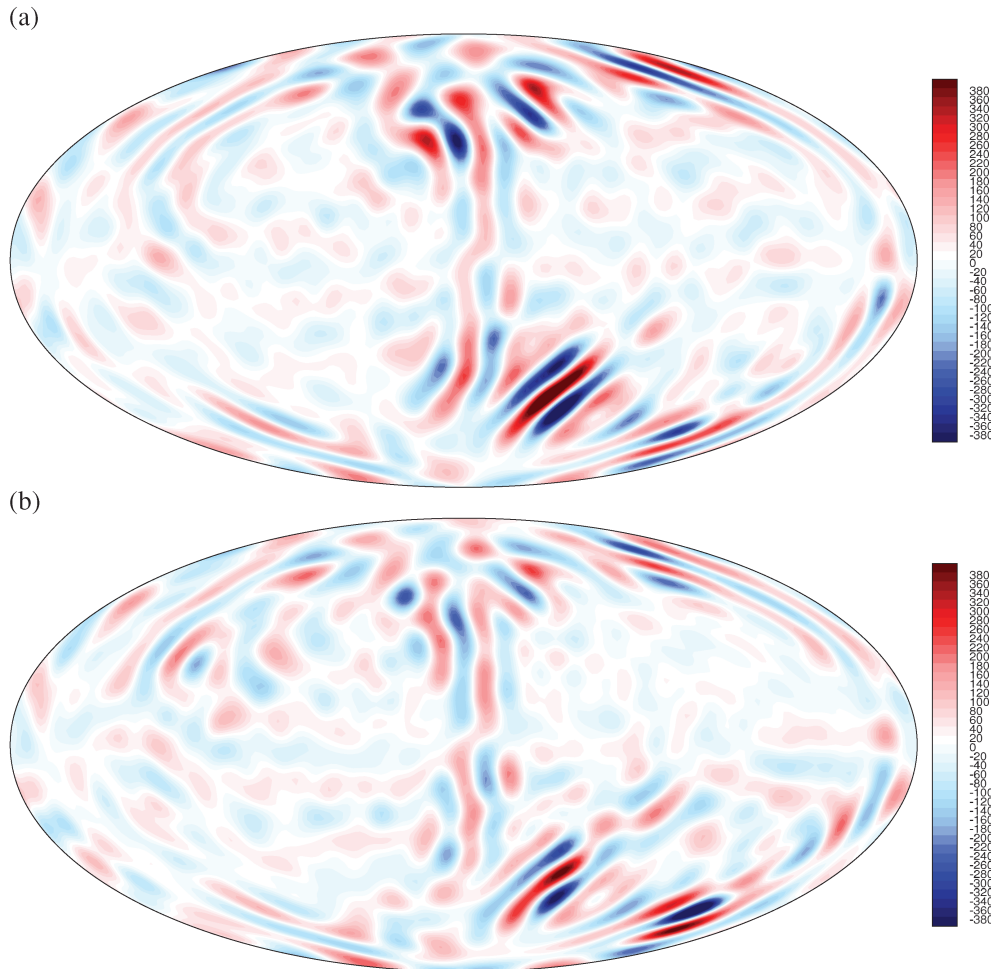
Figure 7. Spatial distribution of the differences between (a) Quadratic model and input model and (b) MaxEnt model and input model. Plotted is B_r in µT.

Table 2. Data, misfit, trade-off parameter λ, entropy S and unsigned flux $\mathcal{N}$ for the 1980 and 2000 MaxEnt models. X, Y and Z are the north, east and down components of the magnetic field. A 'default' value of $d_i = 10$ µT has been used; this small value does not unduly penalize large amplitude features.

Model	No. of data	Misfit= $\sqrt{\chi^2/N}$	λ	S (µT)	$\mathcal{N}$ (mT)
1980	1600 (Z)	1.00	3.82×10^{-2}	-873×10^3	2.91
2000	3684 (X,Y,Z)	1.00	2.50×10^{-2}	-865×10^3	2.90

Jackson (2003). This value is small enough to avoid the behaviour described in Paper II, namely that the method becomes equivalent to the quadratic regularization method when the default d is large compared to the typical amplitudes required in the image by the data. Paper II gives a discussion of the effects of chosing different d on the spherical harmonic spectra. There appears to be no way of deriving what d should be *a priori*. In a synthetic experiment, one can of course discover what the optimal value of d would be, such that the results of the inversion are optimal. We have not done that, nor do we see great value in doing so; when faced with analysing real data, there is no way of checking what the correct answer should be, and it is unlikely that the 'best' default value corresponds to the optimal value found when analysing a synthetic dynamo model. For the dynamo model analysed here, one does in fact obtain superior results with a slightly different default: for $d = 30$ µT the standard deviations of the residuals drops to 67.4 µT (recall the values for the $d = 10$ µT MaxEnt model and the quadratically regularized model

were 70.2 and 78.8 µT, respectively). The problem remains open to further study.

4.2 Application to satellite data

We now apply the method to two high-quality data sets; some results previously appeared in Jackson (2003), but we give more details of the parameters used for the inversion, and compare with the synthetic example. The first is a selection of Magsat data from 1980, used previously by Shure *et al.* (1985). Only Z data up to $\pm 83°$ latitude are used. The second is from the satellite Ørsted, used previously by Olsen *et al.* (2000) to create the Ørsted Initial Field Model; the selection of data is from December 1999–January 2000. It has been reduced to epoch using the IGRF secular variation model, and had the external field of Olsen *et al.* (2000) removed. In calculating the models the Magsat data are assigned errors of
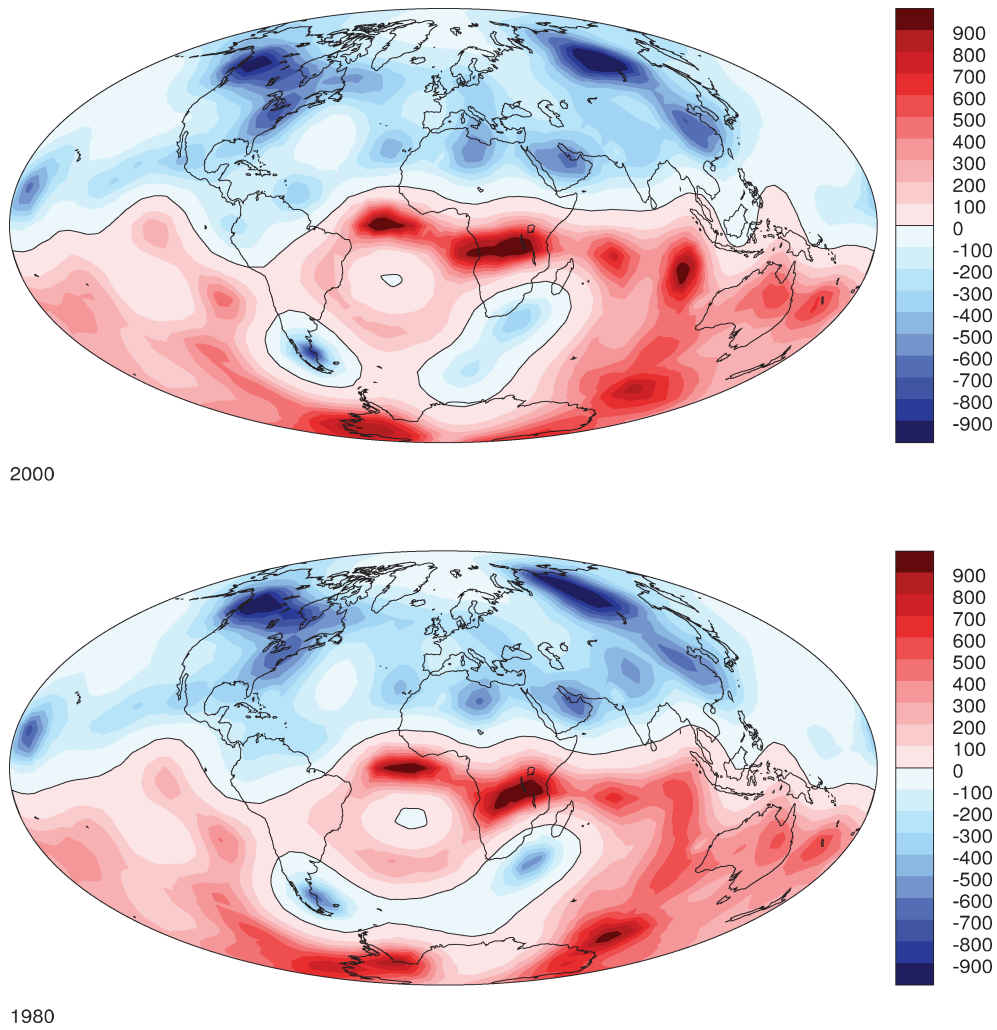
Figure 8. Comparison of the radial magnetic field for epochs 1980 and 2000 on Aitoff equal-area projection. Red colours represent magnetic flux out of the core, while blue colours represent magnetic flux entering the core; each colour bar represents an interval of 100 µT. The continental outlines are for orientation. A 1442-node tesselation has been used.
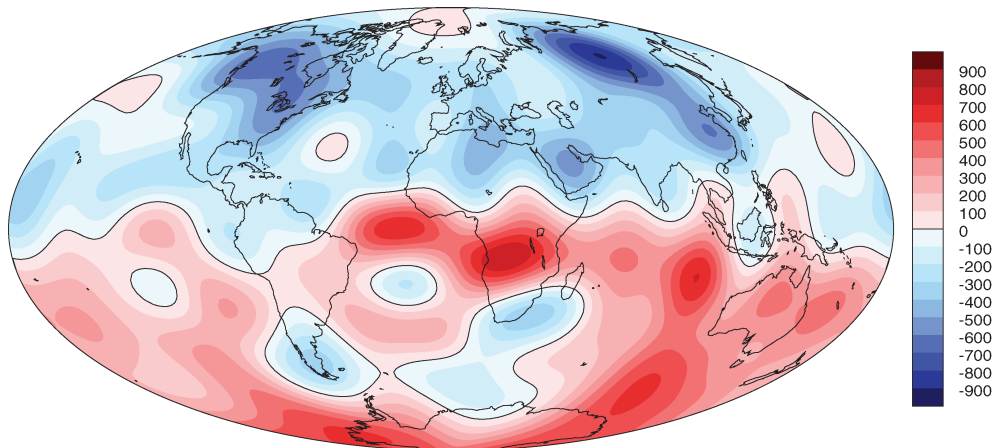
Figure 9. The radial magnetic field for epoch 2000 on Aitoff equal-area projection, constructed using conventional quadratic regularization. The misfit is the same as that of the maximum entropy model of Fig. 8. Red colours represent magnetic flux out of the core, while blue colours represent magnetic flux entering the core; each colour bar represents an interval of 100 µT. The continental outlines are for orientation.

10 nT, commensurate with previous studies. The Ørsted data have lower errors and are treated using the anisotropic error model of Holme & Bloxham (1996); we use $\sigma = 2.25$ nT, and errors of $10''$ and $60''$ for the two pointing angle errors (Olsen *et al.* 2000). We invert these data sets using the same value of the default parameter as that used in the simulation. Details of the models are given in Table 2.

The values for the negentropy are a little less than 10 per cent different to that found for the simulated data set. We report values of the unsigned flux $\mathcal{N}$ given by

$$\mathcal{N} = \int_\Omega |B_r| \, d\Omega. \tag{20}$$

It is interesting that the unsigned flux of the two models differs by less than 0.5 per cent. Although it is possible to do so, the monopole component is not explicitly constrained to be zero, but we find *a posteriori* that it is naturally satisfied to better than one part in 10^5.

Fig. 8 shows the fields on the core surface separated by 20 yr. These models illustrate the intense equatorial spots on the core surface previously highlighted by Jackson (2003). Of particular note in these maps are the locations where the radial flux changes sign— the so-called null-flux curves on which $B_r = 0$. These contours are of importance because they bound regions, the so-called null flux patches, which under the theory of frozen flux (Roberts & Scott 1965), should retain the same amount of flux throughout time. What is noteworthy is how simple these maps are in terms of their null-flux curve topology. Although the location and number of null-flux curves is notoriously hard to determine, even with a high-quality data set (O'Brien 1996), most maps of the core field for 1980 or 2000 have on the order of 8–10 null flux curves (e.g. Fig. 9), whereas our results for 1980 has only three curves and the result for 2000 has four. This has implications for models that attempt to conserve flux, as the number of constraints is then drastically reduced. Note that there is no longer a null-flux curve at the north pole as occurs in quadratically damped models. In many ways it is the smoothly decaying power spectrum that allows this level of 'simplicity' in the models.

Fig. 10 shows the spherical harmonic energy spectrum of the result for 1980 (often called the Lowes spectrum). These spectra are much more realistic when compared to numerical dynamo model output, such as that shown in Fig. 4, which shows a very slow decrease of magnetic energy with increasing spherical harmonic degree.

5 DISCUSSION

We have presented the foundations of the maximum entropy method and its application to a deconvolution problem in geomagnetism, but the applications of the method in geophysics could be much broader. Many problems in seismology are faced with 'images' which are known to have high dynamic range, because of the nature of the underlying structures (e.g. slabs in seismic tomography). For this reason we suggest that it is a technique that warrants more attention in all areas of imaging in geoscience: seismology and environmental geophysics are immediate areas of application. The idea, originating with Gull & Skilling (1990), of having two underlying images each of which is a PAD from which the whole image is constructed, allows the application of the technique to problems where there is no obvious positivity in the image. This enlarges the scope of the method to an extremely large class of problems.
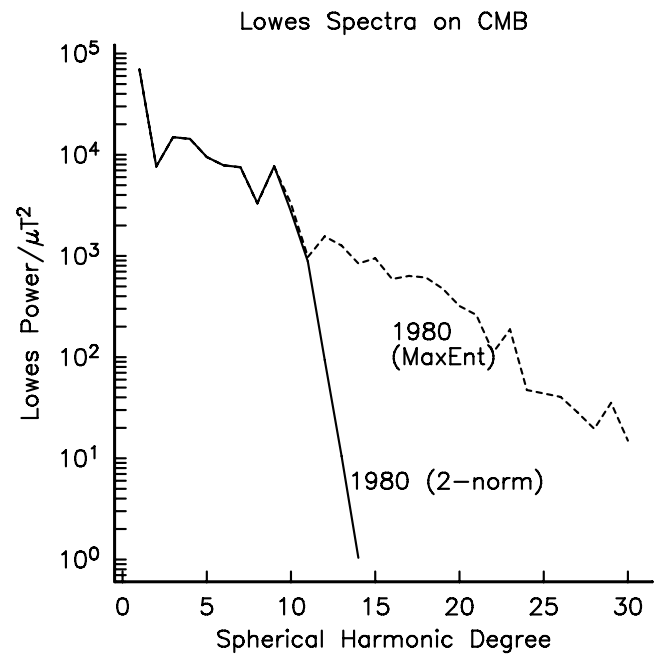
Figure 10. Comparison of the spherical harmonic energy (Lowes) spectrum (the contribution by spherical harmonic degree to $|\mathbf{B}|^2$) on the core surface for conventional 2-norm model and maximum entropy model.

REFERENCES

Backus, G.E., 1988. Bayesian inference in geomagnetism, *Geophys. J.,* **92,** 125–142.

Backus, G.E. & Gilbert, F., 1967. Numerical applications of a formalism for geophysical inverse problems, *Geophys. J. R. astr. Soc.,* **13,** 247–276.

Backus, G.E., Parker, R. & Constable, C., 1996. *Foundations of Geomagnetism*, Cambridge University Press, Cambridge.

Baumgardner, J. & Fredrickson, P.O., 1985. Icosahedral discretization of the two-sphere, *SIAM J. Num. Anal.,* **22,** 1107–1115.

Buck, B. & Macaulay, V.A. (Eds), 1991. *Maximum Entropy in Action*, Oxford University Press, Oxford.

Christensen, U., Olsen, P. & Glatzmaier, G.A., 1999. Numerical modelling of the geodynamo: a systematic parameter study, *Geophys. J. Int.,* **138,** 393–409.

Constable, C.G., Parker, R.L. & Stark, P.B., 1993. Geomagnetic field models incorporating frozen-flux constraints, *Geophys. J. Int.,* **113,** 419–433.

David, W.I.F., 1990. Extending the power of powder diffraction for structure determination, *Nature,* **346,** 731–734.

Gillet, N., Jackson, A. & Finlay, C.C., 2007. Maximum entropy regularization of time-dependent geomagnetic field models, *Geophys. J. Int.,* doi: 10.1111/j.1365-246X.2007.03521.x

Gubbins, D. & Roberts, N., 1983. Use of the frozen flux approximation in the interpretation of archæomagnetic and palæomagnetic data, *Geophys. J. R. astr. Soc.,* **73,** 675–687.

Gull, S.F. & Skilling, J., 1990. The MEMSYS5 User's Manual. Maximum Entropy Data Consultants Ltd., Royston. http://www.maxent.co.uk/documents/MemSys5_manual.pdf

Holme, R. & Bloxham, J., 1996. The treatment of attitude errors in satellite geomagnetic data, *Phys. Earth planet. Int.,* **98,** 221–233.

Hobson, M.P. & Lasenby, A.N., 1998. The entropic prior for distributions with positive and negative values, *Mon. Not. R. Astron. Soc,* **298,** 905–908.

Jackson, A., 2003. Intense equatorial flux spots on the surface of Earth's core, *Nature* **424,** 760–763.

Jaynes, E.T., 2003. *Probability Theory, the Logic of Science*, ed. Bretthorst, G.L., Cambridge Univ. Press, Cambridge.

Maisinger, K., Hobson, M.P. & Lasenby, A.N., 1997. A maximum entropy method for reconstructing interferometer maps of fluctuations in the cosmic microwave background radiation, *Mon. Not. R. Astron. Soc,* **290,** 313–326.

Maus, S., Rother, M., Hemant, K., Luhr, H., Kuvshinov, A. & Olsen, N., 2006. Earth's lithospheric magnetic field determined to spherical harmonic degree 90 from CHAMP satellite measurements, *Geophys. J. Int.,* **164,** 319–330.

O'Brien, M.S., 1996. Resolving magnetic flux patches at the surface of the core, *Geophys. Res. Lett.,* **23,** 3071–3074.

Olsen, N. & members of the Ørsted International Science Team, 2000. Ørsted Initial Field Model, *Geophys. Res. Lett.,* **27,** 3607–3610.

Paige, C.C. & Saunders, M.A., 1982. LSQR: an algorithm for sparse linear equations and sparse least squares, ACM Trans. Math. Soft., **8,** 43–71.

Parker, R.L., 1994. *Geophysical Inverse Theory*, Princeton University Press, Princeton.

Roberts, P.H. & Scott, S., 1965. On analysis of the secular variation. 1. A hydromagnetic constraint: theory, *J. Geomagn. Geoelectr.,* **17,** 137–151.

Sambridge, M.S., Braun, J. & McQueen, H., 1995. Geophysical prametrization and interpolation of irregular data using natural neighbours, *Geophys. J. Int.,* **122,** 837–857.

Shure, L., Parker, R.L. & Langel, R.A., 1985. A preliminary harmonic spline model from Magsat data, *J. geophys. Res.,* **90,** 11 505–11 512.

Sivia, D.S. & Skilling, J., 2006. *Data Analysis. A Bayesian Tutorial*, Oxford University Press, Oxford.

Skilling, J., 1998. Massive inference and maximum entropy, in *Maximum Entropy and Bayesian Methods*, eds Fisher R., Preuss, R. & von Toussaint, U., Kluwer, Dordrecht.

Skilling, J. & Bryan, R.K., 1984. Maximum entropy image reconstruction: general algorithm, *Mon. Not. R. Astron. Soc,* **211,** 111–124.

Tarantola, A., 1987. *Inverse Problem Theory. Methods for Data Fitting and Model Parameter Estimation*, Elsevier, Amsterdam, 613p.

Tarantola, A. & Valette, B., 1982a. Generalized nonlinear inverse problems solved using the least squares criterion, *Rev. Geophys. Space Phys.,* **20,** 219–232.

Tarantola, A. & Valette, B., 1982b. Inverse problems = Quest for information, *J. Geophys.,* **50,** 159–170.